Received: 23 May 2021 | Accepted: 25 September 2021

DOI: 10.1111/srt.13111

ORIGINAL ARTICLE

WILEY

Automatic segmentation and melanoma detection based on color and texture features in dermoscopic images

S. Oukil[1] | R. Kasmi[1,2] | K. Mokrani[1] | B. García-Zapirain[3]

[1] LTII Laboratory University of Bejaia-Algeria, Faculty of Technology, University of Bejaia, Bejaia, Algeria

[2] Electrical Engineering Department, University of Bouira, Bouira, Algeria

[3] eVIDA Research Group, University of Deusto, Bilbao, Spain

Correspondence
Reda Kasmi, Electrical Engineering Department U Bouira, LTII Laboratory University of Bejaia-Algeria, Faculty of Technology, University of Bejaia, 06000 Bejaia, Algeria.
Email: rdkasmi@gmail.com

Abstract

Purpose: Melanoma is known as the most aggressive form of skin cancer and one of the fastest growing malignant tumors worldwide. Several computer-aided diagnosis systems for melanoma have been proposed, still, the algorithms encounter difficulties in the early stage of lesions. This paper aims to discriminate melanoma and benign skin lesion in dermoscopic images.

Methods: The proposed algorithm is based on the color and texture of skin lesions by introducing a novel feature extraction technique. The algorithm uses an automatic segmentation based on *k*-means generating a fairly accurate mask for each lesion. The feature extraction consists of the existing and novel color and texture attributes measuring how color and texture vary inside the lesion. To find the optimal results, all the attributes are extracted from lesions in five different color spaces (RGB, HSV, Lab, XYZ, and YCbCr) and used as the inputs for three classifiers (*K* nearest neighbors, support vector machine , and artificial neural network).

Results: The PH2 set is used to assess the performance of the proposed algorithm. The results of our algorithm are compared to the results of published articles that used the same dataset, and it shows that the proposed method outperforms the state of the art by attaining a sensitivity of 99.25%, specificity of 99.58%, and accuracy of 99.51%.

Conclusion: The final results show that the colors combined with texture are powerful and relevant attributes for melanoma detection and show improvement over the state of the art.

KEYWORDS
classification, dermoscopy, features extraction, *K*-means, melanoma, segmentation, super-pixel

1 | INTRODUCTION

Skin cancer is an uncontrolled growth of skin cells. Melanoma is the most dangerous form of skin cancer. The American Cancer Society estimates 106 110 cases, and 7180 likely will pass away from melanoma in 2021.[1] When detected and treated at its early stage, melanoma is not a threat to life, in this case, computer-assisted treatment is the obvious solution.[2,3] Numerous computer-aided diagnosis systems for melanoma have been proposed based on deep learning features[4–7] or handcrafted features.[8–11] Kasmi and Mokrani[12] proposed an automatic detection based on the ABCD rule features. Tested on 200 dermoscopic images, the algorithm achieves a sensitivity rate of 91.25%, a precision of 95.83%, and an accuracy of 94.0%. Jaworek-Korjakowska et al.[13] used the shape and texture of

the lesion to detect melanoma at its early stage with the support vector machine (SVM) classifier. A set of 200 images is used and reported a sensitivity of 90%, specificity of 96%, and the area under the curve equal to 93.24%. In the paper of Barata et al.,[14] a Bag-of-features is used, the study compares the weight of color and texture descriptors for melanoma. The method achieves a sensitivity of 93% and a specificity of 88%. Alfed et al.[15] combine texture (histogram of gradients, histogram of lines) with color vector angles and Zernike moments as features to classify melanoma from benign lesions of PH2 dataset,[16,17] using three classifiers SVM, Adaboost, and artificial neural network (ANN). The method achieves the sensitivity of 99.41% and specificity of 98.18% and accuracy of 98.79%. Majumder et al.[18] based on the ABCD rule features, a back-propagation neural network is used to classify melanomas from benign on PH2 dataset.[16,17] The results determine the overall accuracy of 98%. Abbas et al.[19] proposed a novel pattern classification method based on color symmetry and multiscale texture analysis, by developing AdaBoost.MC multilabel algorithm. The classification results obtained a sensitivity (SE) of 89.28%, specificity (SP) of 93.75%, and an area under the curve of 0.986. Hagerty et al.[20] mix the handcrafted and deep learning features after assessing them individually. The study shows the effectiveness of the fusion features by obtaining a classification accuracy of 0.94. Moura et al.[21] use the ABCD rule and pre-trained convolutional neural networks features, and then the most relevant descriptors are chosen. Finally, a MultiLayer Perceptron classifier is used to distinguish melanoma from benign lesions. The method achieved an accuracy rate of 94.9% and a Kappa index of 89.2%. Hirano et al.[22] developed an automated melanoma diagnosis system using hyperspectral data (HSD) and GoogLeNet. The pre-formed GoogLeNet is used to power the HSD, they added a new network, called "mini network," which performs a size reduction just before the input layer of GoogLeNet. The work used 619 lesions for training and testing. The evaluation on five cross-validations indicates that without data augmentation, the sensitivity, specificity, and accuracy are 69.1%, 75.7%, and 72.7%, respectively. And with data augmentation, the sensitivity, specificity, and accuracy are 72.3%, 81.2%, and 77.2%, respectively. Acosta et al.[23] proposed melanoma classification method consists of two steps: first, the region of interest is cropped using mask and region-based convolutional neural network technique. Second, a classifier based on the ResNet152 structure is used to discriminate malignant lesions. The method is assessed on the ISIC2017 set and achieves an accuracy of 90.4%, sensitivity of 82%, and specificity of 92.5%.

This work aims to find an accurate algorithm for melanoma recognition based on the color and texture features. First, we proposed a segmentation algorithm that localizes lesions. Then, we extracted novel and representative features that measure the color and texture variations in the lesion. The method is tested on the PH2 public set.[16,17] To find an optimal result, we assessed the algorithm in different configurations combining different color spaces and different classifiers. The results of our method are compared to the published results using the same dataset.

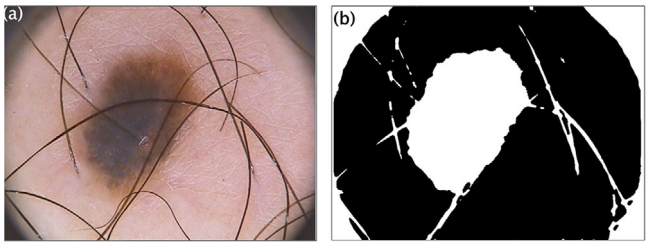

FIGURE 1 Lesion segmentation (A): original image (B) *k*-means segmentation

2 | LESION SEGMENTATION

The lesion segmentation is one of the most important steps for an efficient classification of lesions using handcrafted features. In this work, the *K*-means[24,25] technique is used to localize lesions. It is performed either on a green color plane (G), after adjustment of its histogram and minimizing the effect of hair by a 11×11 median filter, or on a second new plane that combines the two planes S (saturation) and V (value) of HSV color space.[26] The second plane is found as shown in Equation (1): Because of the weak boundaries of lesions, the contour detection methods can not delimit the lesions well using the known planes (R, G, B, H, S V,…). So a combination of planes that highlight the lesion is recommended. In this case, the intensity of color S and the brightness V are combined with reducing the both values (S x0.9) and (V x 0.3).

Knowing that the lesion is more colorful less bright than the background, the combination of the S and reduced V planes makes the lesion brighter and the background darker. This is what helps the k-means to segment easily the lesions.

$$\text{Inew} = \begin{cases} (0.9S + 0.3V) \text{ if } (0.9S + 0.3V) < 1 \\ 1 \text{ otherwise} \end{cases} \quad (1)$$

The choice of the plane is based on the standard deviation of the green plane (std(G)). We noticed that if the standard deviation of the green plane G is higher than 0.25, the lesion is highlighted enough to be segmented by k-means, otherwise we use the plane found by equation 1.

$$I = \begin{cases} Inew \text{ if } std\,(G) < 0.25 \\ G \text{ otherwise} \end{cases} \quad (2)$$

Figure 1 shows the lesion segmentation using *K*-means with $K = 2$.

2.1 | Post-processing of *K*-means segmentation

Vignetting in some images is seen and kept as a part of the lesion as shown in Figure 1B. The non-lesion objects are either from hair or from the dark corners of the image. The corner removal consists of detecting the dark corners alone and then removes them from the *k*-means

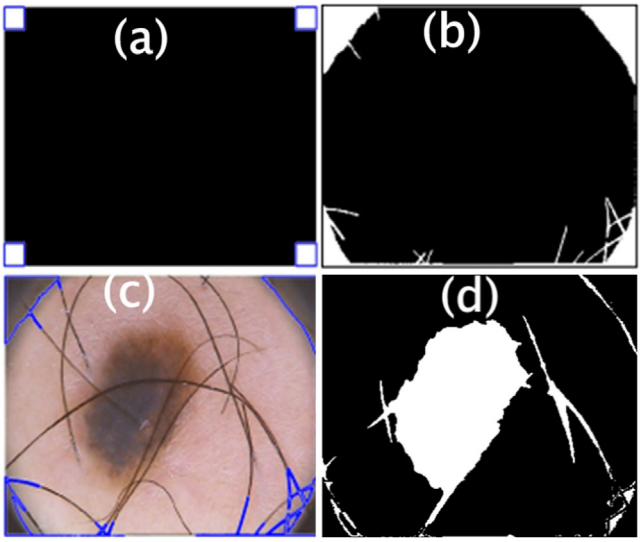

FIGURE 2 Corner segmentation by active contours (A) contour initialization (B) detected corners (C) overlay contour on the original image (d) lesion mask after removing corners

mask. The corners are segmented using active contours[27,28] that is based on the evolution model (Equation (3)). An initial contour C moves toward the edges and stops by the decreasing function g (Equation (4)).

The evolution of each point of the contour $C(t)$ with velocity V in the normal direction is computed as the curvature motion in the normal direction $K\vec{N}$. The decreasing function (Equation (4)) depends on one over a gradient of the image. In the contours, the gradient is high, which makes the decreasing function tend to zero at the edges. Multiplying the decreasing function by the curvature motion stops the contour evolution at the edges. And because the lesion's contours are most of the time not sharp, the second term of Equation (3), projected in the normal direction, is an additional stopping function.

$$\frac{\partial C(t)}{\partial t} = \left(g(I)k - \left\langle \nabla g(I), \vec{N} \right\rangle\right)\vec{N} \tag{3}$$

$$g(I) = \frac{1}{1 + (\nabla I)^2} \tag{4}$$

where:

C: contour;
∇I: Gradient of the grayscale of the plane I;
k: Curvature;

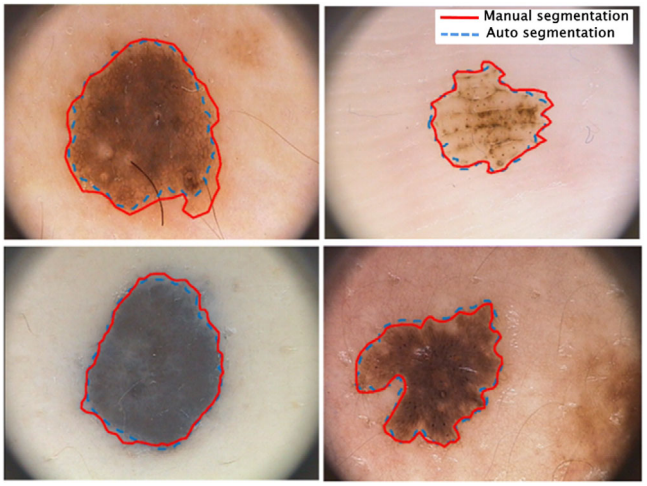

FIGURE 4 Lesions segmentation: Overlay automatic and manual contours

$\vec{N}$: Unit vector in the normal direction;
$\langle \nabla g(I), \vec{N} \rangle \vec{N}$: The inner product, projection of the gradient of the stopping function in the normal direction.

Figure 2 shows the corner detection using the active contours method and the lesion mask after removing corners.

To remove the non-lesion area, all the objects with an area smaller than 700 pixels are eliminated. Then, the objects are eroded using morphological operation erosion with a structural element of disk radius equal to 10, followed by dilatation using a structural element of disk with a radius equal to 15. The filtering steps are shown in Figure 3.

2.2 | Results and comparison of the segmentation

The automatic segmentation generates an accurate mask for each lesion. Figure 4 shows some results of the proposed segmentation method. The manual contour (continuous line) and automatic contour (dashed line) are overplayed.

The automatic segmentation results are compared to the results reported in the published paper of Jaisakthi et al.[29] where the author proposed an algorithm of segmentation tested on the PH2 dataset. Five metrics are used to assess the segmentation results: sensitivity, specificity, accuracy, dice, and Jaccard.

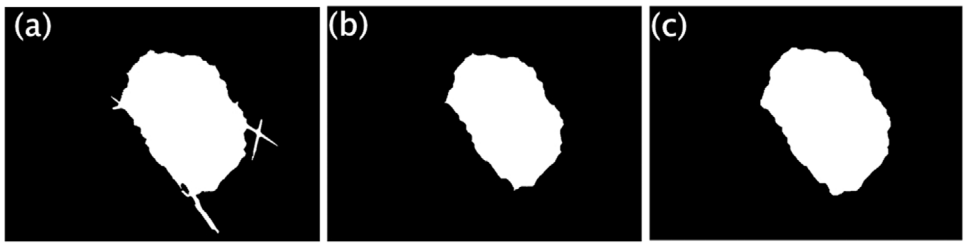

FIGURE 3 Filtering (A) lesion mask with extra objects (B) erosion (C) dilatation, and final mask

TABLE 1 Segmentation results and comparison

Metrics	Jaisakthi et al[29]	Our algorithm
Accuracy	0.9604	0.9606
Sensitivity	0.8900	0.9236
Specificity	0.9879	0.9870
Dice	0.9139	0.9167
Jaccard	0.8437	0.8462

$$\text{Sensitivity} = \frac{TP}{TP + FN} \quad (5)$$

$$\text{Spesificity} = \frac{TN}{TN + FP} \quad (6)$$

$$\text{Accuracy} = \frac{TP + TN}{TP + TN + FP + FN} \quad (7)$$

$$\text{Dice} = \frac{TP}{\left(TP + \frac{FP+FN}{2}\right)} \quad (8)$$

$$\text{Jacard} = \frac{TP}{TP + FP + FN} \quad (9)$$

where TP is the true positive, TN is the true negative. FP is the false positive. FN is the false negative.

Table 1 shows the comparison of the results of the segmentation.

The proposed segmentation algorithm generates a mask for each lesion close enough to the manual segmentation; they are used to extract features presented in the following section.

3 | FEATURE EXTRACTION

The presence of multicolor and non-homogeneity in the lesion is the most important sign of malignancy.[30,31]

3.1 | Quantify frequent color

After visual inspection of all lesions in the PH2 dataset, we conclude that there are, subjectively, six dominant colors, we named: light brown, mid-brown, dark brown, black, white, and blue-gray, which we need to quantify. To measure the averages of the six dominant colors in the lesions, the images are over segmented using super-pixel technique to 900 blobs as shown in Figure 5. Super-pixel is based on a linear iterative clustering algorithm[32] to gather pixels with similar values into a group (blob).

From all super-pixels that visually appear as the same color, we extracted and saved the R, G, and B color values. The operation is repeated for 100 images. A similar procedure is done for six dominant colors, and then we considered the averages are the color references. The results are reported in Table 2.

Once we had the references of the six frequent colors, we measured the color distances of each super-pixel in a given lesion to the six color references mentioned in Table 2 using the Euclidean distance, (Equation (10)).

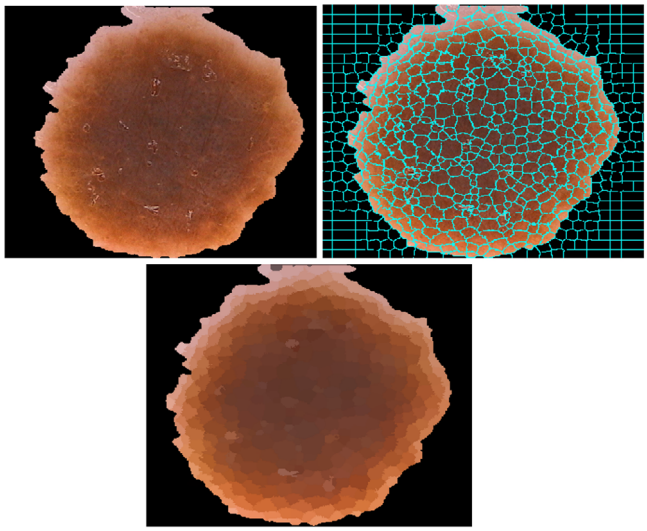

FIGURE 5 Lesion pixilated with a super-pixel algorithm

TABLE 2 The six frequent color references

Color	Appearance	Color references (R_{ref}, G_{ref}, B_{ref})
Light brown		(200, 155, 130)
Mid-brown		(160, 100, 67)
Dark brown		(126, 67, 48)
White		(230, 230, 230)
Black		(31, 26, 26)
Blue-gray		(75, 112, 137)

$$\text{Dist}\ (i) = \sqrt{(R_i - R_{ref})^2 + (G_i - G_{ref})^2 + (B_i - B_{ref})^2} \quad (10)$$

Where,

Dist(i): distance of a given super-pixel *i* to one of the reference colors (Table 2),

R_i, G_i, B_i: red, green, and blue color channel of a super-pixel *i*.

A super-pixel is attributed to a given color if its normalized distance is lower than an empirical threshold T, variable for each color. The thresholds are reported in Table 3.

A given color is considered present only if it occupies an area more than 5% of the lesion area.

The number of colors detected in a given lesion is used as the number of cluster *K* for *K*-means, and the lesion is segmented into *K* classes. Figure 6 shows the classes found by *K*-means.

TABLE 3 Color thresholds to attribute a given super-pixel color

Color	Light brown	Middle brown	Darkbrown	White	Black	Blue Grey
Threshold	0.12	0.25	0.2	0.25	0.25	0.5

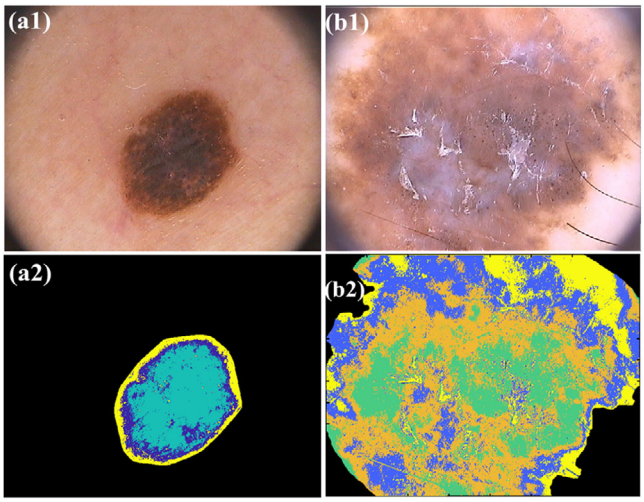

FIGURE 6 *K*-means segmentation. (A) A lesion with three classes. (B) A lesion with four classes

3.2 | Color features

In this section, we reported the equations of the feature that we extracted from the R, G, and B planes of the RGB color space. Same features are extracted from H, S, V planes of HSV color space, L, a, b planes of Lab color space, X, Y, Z planes of XYZ color space, Y, Cb, Cr planes of YCbCr color space, respectively.

The average of red, green, and blue plane (avgR, avgG, avgB) are computed for each class *n*

$$\text{avgR}(n) = \frac{1}{I * J} \sum_{i=1}^{I} \sum_{j=1}^{J} R(i_n, j_n) \tag{11}$$

avgR(n): Average of the class *n* for R plane.
(n = 1 to K)
R: red plane
(i_n, j_n): Coordinates of the pixels of the class *n*.

The C_1, C_2, C_3 are the ratio of the relative colors, considering the maximum average of the *K* classes (Equations (12)–(14))

$$C_1 = \max\left(\frac{\text{avgR}(n)}{R_{skin}}\right)_{n=1..K} \tag{12}$$

$$C_2 = \max\left(\frac{\text{avgG}(n)}{G_{skin}}\right)_{n=1..K} \tag{13}$$

$$C_3 = \max\left(\frac{\text{avgB}(n)}{B_{skin}}\right)_{n=1..K} \tag{14}$$

The C_4, C_5, and C_6 are the normalized relative[33] R, G, and B ratios, considering the classes with maximum average color.

$$C_4 = \frac{C_1}{(C_1 + C_2 + C_3)} \tag{15}$$

$$C_5 = \frac{C_2}{(C_1 + C_2 + C_3)} \tag{16}$$

$$C_6 = \frac{C_3}{(C_1 + C_2 + C_3)} \tag{17}$$

The C_7, C_8, and C_9 are the relative difference[33] R, G, and B, considering classes with maximum average color.

$$C_7 = C_1 - R_{Skin} \tag{18}$$

$$C_8 = C_2 - G_{Skin} \tag{19}$$

$$C_9 = C_3 - B_{Skin} \tag{20}$$

Where: R_{Skin}, G_{Skin}, and B_{Skin} are the averages of red, green, and blue color plane, respectively, of skin surrounding the lesion.

The C_{10}, C_{11}, and C_{12} are the normalized relative difference[33] R, G, B, selecting classes with maximum average color.

$$C_{10} = \frac{C_7}{(C_7 + C_8 + C_9)} \tag{21}$$

$$C_{11} = \frac{C_8}{(C_7 + C_8 + C_9)} \tag{22}$$

$$C_{12} = \frac{C_9}{(C_7 + C_8 + C_9)} \tag{23}$$

C_{13}, C_{14}, and C_{15} we compute the Euclidean color distances between classes for each channel.

$$C_{13} = \sqrt{\sum_{i=n}^{K-1} (\text{avgR}(n) - \text{avgR}(n+1))^2} \tag{24}$$

$$C_{14} = \sqrt{\sum_{i=n}^{K-1} (\text{avgG}(n) - \text{avgG}(n+1))^2} \tag{25}$$

$$C_{15} = \sqrt{\sum_{i=n}^{K-1} (\text{avgB}(n) - \text{avgB}(n+1))^2} \tag{26}$$

C_{16}, C_{17}, and C_{18} are the variances between classes in different color channel.

$$C_{16} = \frac{\sum_{n=1}^{K} \left(\text{avgR}(n) - \overline{\text{avgR}}\right)^2}{K} \tag{27}$$

$$C_{17} = \frac{\sum_{n=1}^{K} \left(\text{avgG}(n) - \overline{\text{avgG}}\right)^2}{K} \quad (28)$$

$$C_{18} = \frac{\sum_{n=1}^{K} \left(\text{avgB}(n) - \overline{\text{avgB}}\right)^2}{K} \quad (29)$$

C_{19}, C_{20}, and C_{21} are the standard deviation between classes in different color channel.

$$C_{19} = \sqrt{C_{16}} \quad (30)$$

$$C_{20} = \sqrt{C_{17}} \quad (31)$$

$$C_{21} = \sqrt{C_{18}} \quad (32)$$

C_{22}, C_{23}, and C_{24} are the variances of the normalized color between classes.

$$\text{avgRD}(n) = |\text{avgR}(n) - R_{Skin}| \quad (33)$$

$$C_{22} = \frac{\sum_{n=1}^{K} \left(\text{avgRD}(n) - \overline{\text{avgRD}}\right)^2}{K} \quad (34)$$

$$\text{avgGD}(n) = |\text{avgG}(n) - G_{Skin}| \quad (35)$$

$$C_{23} = \frac{\sum_{n=1}^{K} \left(\text{avgGD}(n) - \overline{\text{avgGD}}\right)^2}{K} \quad (36)$$

$$\text{avgBD}(n) = |\text{avgB}(n) - B_{Skin}| \quad (37)$$

$$C_{24} = \frac{\sum_{n=1}^{K} \left(\text{avgBD}(n) - \overline{\text{avgBD}}\right)^2}{K} \quad (38)$$

avgR(n), avgG(n), avgB(n): Averages of the class n in red, green, and blue planes, respectively.

n: n'th class ($n = 1$ to K)

$R_{Skin}G_{Skin}$, B_{Skin}: Skin colors that surround the lesion in red, green, and blue planes.

3.3 | Texture features

We compute the Euclidean distances between entropies of classes of the lesion, for each channel, R, G, and B noting, respectively, T_1, T_2, and T_3.

The greater the distance of entropies between classes, the more likely it is a melanoma.

$$T_1 = \sqrt{\sum_{i=n}^{K-1} (\text{EntropyR}(n) - \text{EntropyR}(n+1))^2} \quad (39)$$

$$T_2 = \sqrt{\sum_{i=n}^{K-1} (\text{EntropyG}(n) - \text{EntropyG}(n+1))^2} \quad (40)$$

$$T_3 = \sqrt{\sum_{i=n}^{K-1} (\text{EntropyB}(n) - \text{EntropyB}(n+1))^2} \quad (41)$$

EntropyR(n), Entropy$G$(n), Entropy$B$(n): Entropy of the n'th class in the red, green, and blue plane respectively. The three characteristics are measured from the first plane for each color space (R, H, X, and Y).

Then, we used the cooccurrence matrix by fixing the range of [0 1] between pixels, to measure three properties: contrast, homogeneity, and energy. The three properties are measured from the first plane for each color space (R, H, X, and Y).

$$T_4 = \text{Contrast} = \sum_{i}^{M} \sum_{j}^{N} |i-j|^2 G(i,j) \quad (42)$$

$$T_5 = \text{Homogeneity} = \sum_{i}^{M} \sum_{j}^{N} \frac{G(i,j)}{1+|i-j|} \quad (43)$$

$$T_6 = \text{Energy} = \sum_{i}^{M} \sum_{j}^{N} G(i,j)^2 \quad (44)$$

G : Cooccurrence matrix of the H plane (hue)

M, N: Cooccurrence matrix dimension.

4 | RESULTS AND DISCUSSION

4.1 | Dataset

In this work, we used the PH2 dataset which is a public set intended for research and benchmarking.[16,17] It contains 200 dermoscopic images, where 80 common nevi, 80 atypical nevi, and 40 melanomas. The PH2 dataset includes manual segmentation for each lesion.

For the classification, all the features are extracted using our automatic masks.

4.2 | Features selection

Before classification, we select the most discriminative features by the relief method[34] from all extracted color and texture features. The Relief algorithm attributes a score for each feature according to its importance.

4.3 | Classification

To find the optimum configuration between the classifiers and the color spaces, we extracted the same features from RGB, HSV, Lab, XYZ, and

TABLE 4 Classification of melanoma and benign lesions using different classifiers and color spaces on PH2 set

Color space	Features	KNN			ANN			SVM		
		SE (%)	SP (%)	ACC (%)	SE (%)	SP (%)	ACC (%)	SE (%)	SP (%)	ACC (%)
RGB	T1, T3, T2, T4, T5, C13, C11, C2	99.23	98.26	98.46	98.25	99.45	99.2	**99.25**	**99.58**	**99.51**
HSV	T1, T2, T3, C22, C13, C16, C19, T4	95.73	99.11	98.44	92.25	99.45	98	94.92	99.55	98.62
LAB	T12, T4, T5,T16, C4, C7	94	98.81	97.85	95.25	98.02	97.45	95.71	96.19	96.09
XYZ	C15, T4, C21, C14, C18, T5, T3, C21	91.66	95.13	94.44	84	97.02	94.4	90.83	96.87	95.66
YCbCr	T2, T3, T4, T1, T5, T6, C15, C21, C13	99.21	98.81	98.98	98.5	99.82	99.55	98.8	99.2	99.12

Abbreviations: Acc, accuracy; ANN, artificial neural network; HSV, Hue Saturation and Value; KNNs, *K* nearest neighbors; LAB, lightness and A and B are chromaticity coordinates; RGB, red green and blue; SE, sensitivity; SP, specificity; XYZ, X is a combination of the R, G and B planes Y is the luminance, Z is equivalent to blue; YCbCr, Y is the brightness (luma), Cb is blue minus luma (B-Y) and Cr is red minus luma (R-Y).

YCbCr. And then, used three classier *K* nearest neighbors (KNNs), ANN, and the SVM. The performance of the proposed algorithm is assessed using three metrics, namely SE, SP, and accuracy (ACC), (Equations (5) to (7)).

The test using the PH2 set is to identify melanomas from the benign lesion (atypical nevus common nevus). Measuring the average of 10 cross-validations for each configuration (system color/classifier), the results are reported in Table 4. The features are sorted according to their pertinence.

For the two classifiers (KNN and ANN), the best result is found on the YCbCr color space with nine attributes: six texture attributes (T_2, T_3, T_4, T_1, T_5, T_6) and three color attributes (C_{15}, C_{21}, C_{13}). The KNN uses one sample for testing and the remained samples for training, reach 99.21% of sensitivity, 98.81% of specificity and 98.98% of accuracy. The ANN uses 60% of a lesion for learning and 40% for testing, reaches 99.5% of sensitivity, 99.45% of specificity, and 99.55% of accuracy.

With SVM, the best result is found on the RGB color space with eight attributes: five texture attributes (T_1, T_3, T_2, T_4, T_5) and three color attributes (C_{13}, C_{11}, C_2). Using 60% of a lesion for learning and 40% of a lesion for testing, the classification result reaches 99.25% of sensitivity, 99.58% of specificity, and 99.51% of accuracy.

The three classifiers give good results using a fusion of features. We notice that besides XYZ, texture features are selected as the most relevant for RGB, HSV, Lab, and YCbCr.

Table 5 shows a comparison between the state of the art with best results of our algorithm, found using the same dataset (PH2). Overall, our system outperforms all other methods.

Alfed's method[15] found good results by reaching the sensitivity of 99.4% (our: 99.25%) and accuracy of 98.79% (our: 99.51%). Our algorithm shows the best balance between sensitivity and specificity.

Several papers show that the presence of multiple colors in lesion presents an important biomarker of malignancy.[35–39] In our work, the lesion is divided into *K* classes, where *K* is the number of colors constituting the lesion. And these repartitions are used to extract features. The most selected as relevant features, either the texture or the color features, are measuring the disorder or the variation between the classes. This is coherent with the uncontrolled growth of melanomas.

TABLE 5 Comparison of the classification results of our method to three published methods

Method and year of publication	SE %	SP %	Acc %
Barata,[14] 2014	93	88	–
Alfed,[15] 2017	99.4	98.18	98.79
Majumder,[18] 2018	95	98.8	98
Our method	99.25	99.58	99.51

Abbreviations: Acc, accuracy; SE, sensitivity; SP, specificity.

5 | CONCLUSION

In this article, an efficient system for melanoma detection is presented. The approach includes an automatic segmentation of the lesions based on the *k*-means technique. Dominate color references are found manually from over-segmentation of lesions using super-pixels segmentation. The lesion is divided into classes according to the number of colors constituting the lesion. And these repartitions are used to extract numerous color and texture features, and then the algorithm selects the most relevant features. To find the optimum results, the algorithm is assessed in different configurations, combining five color spaces (RGB, HSV, Lab, XYZ, and YCrCb) and three classifiers (KNN, SVM, and ANN). The public PH2 set intended for research and benchmarking is used to assess the proposed algorithm. It contains 200 dermoscopic images, where 160 benign lesions, and 40 melanomas. The results show that the proposed algorithm is accurate and very sensitive in

identifying melanomas by reaching the sensitivity of 99.25%, specificity of 99.58%, and accuracy of 99.51% with the SVM classifier and RGB color space. The Algorithm shows also good results with different color spaces and different classifiers, obtaining the best results compared to the state of the art. The experiment shows the feasibly of detecting melanomas in different color spaces.

ORCID

R. Kasmi https://orcid.org/0000-0003-0898-3382
B. García-Zapirain https://orcid.org/0000-0002-9356-1186

REFERENCES

1. Siegel RL, Miller KD, Fuchs HE, Jemal A. Cancer statistics, 2021. CA Cancer J Clin. 2021;71(1):7–33.
2. Birkenfeld JS, Tucker-Schwartz JM, Soenksen LR, Avilés-Izquierdo JA, Marti-Fuster B. Computer-aided classification of suspicious pigmented lesions using wide-field images. Comput Methods Programs Biomed. 2020;195:105631.
3. Barata C, Celebi ME, Marques JS. A survey of feature extraction in dermoscopy image analysis of skin cancer. IEEE J Biomed Health Inform. 2018;23(3):1096–109.
4. Codella NCF, Nguyen Q-B, Pankanti S, Gutman DA, Helba B, Halpern AC, et al. Deep learning ensembles for melanoma recognition in dermoscopy images. IBM J Res Dev. 2017;61(4/5):5:1–5:15.
5. Li Y, Shen L. Skin lesion analysis towards melanoma detection using deep learning network. Sensors 2018;18(2):556.
6. Nida N, Irtaza A, Javed A, Yousaf MH, Mahmood MT. Melanoma lesion detection and segmentation using deep region based convolutional neural network and fuzzy C-means clustering. Int J Med Inf. 2019;124:37–48.
7. Mishra NK, Celebi ME. An overview of melanoma detection in dermoscopy images using image processing and machine learning. arXiv preprint arXiv:1601.07843, 2016.
8. Hameed N, Shabut AM, Ghosh MK, Hossain MA. Multi-class multi-level classification algorithm for skin lesions classification using machine learning techniques. Expert Syst Appl. 2020;141:112961.
9. Celebi ME, Kingravi HA, Uddin B, Iyatomi H, Alp Aslandogan Y, Stoecker, WV, et al. A methodological approach to the classification of dermoscopy images. Comput Med Imaging Graph. 2007;31(6):362–73.
10. Garg N, Sharma V, Kaur P. Melanoma skin cancer detection using image processing. In: Sensors and image processing. Berlin, Germany: Springer; 2018. p. 111–9.
11. Abbas Q, Emre Celebi M, Fondón I. Computer-aided pattern classification system for dermoscopy images. Skin Res Technol. 2012;18(3):278–89.
12. Kasmi R, Mokrani K. Classification of malignant melanoma and benign skin lesions: implementation of automatic ABCD rule. IET Image Proc. 2016;10(6):448–55.
13. Jaworek-Korjakowska J. Computer-aided diagnosis of micro-malignant melanoma lesions applying support vector machines. Biomed Res Int. 2016;2016:1–8.
14. Barata C, Ruela M, Mendonça T, Marques JS. A bag-of-features approach for the classification of melanomas in dermoscopy images: the role of color and texture descriptors. In: Computer vision techniques for the diagnosis of skin cancer. Berlin, Germany: Springer; 2014. p. 49–69.
15. Alfed N, Khelifi F. Bagged textural and color features for melanoma skin cancer detection in dermoscopic and standard images. Expert Syst Appl. 2017;90:101–10.
16. Mendonça T, Ferreira PM, Marques JS, Marcal AR, Rozeira J. PH2-A dermoscopic image database for research and benchmarking. Paper presented at: 2013 35th Annual International Conference of the IEEE Engineering in Medicine and Biology Society (EMBC); July 3-7, 2013; Osaka, Japan.
17. Celebi ME, Mendonça T, Marques JS. Dermoscopy image analysis. Boca Raton: CRC Press; 2016.
18. Majumder S, Ullah MA. Feature extraction from dermoscopy images for an effective diagnosis of melanoma skin cancer. Paper presented at: 2018 10th International Conference on Electrical and Computer Engineering (ICECE); December 20-22, 2018; Dhaka.
19. Abbas Q, Celebi ME, Serrano C, Garcia IF, Ma G. Pattern classification of dermoscopy images: a perceptually uniform model. Pattern Recognit. 2013;46(1):86–97.
20. Hagerty JR, Stanley RJ, Almubarak HA, Lama N, Kasmi R, Guo P, et al. Deep learning and handcrafted method fusion: higher diagnostic accuracy for melanoma dermoscopy images. IEEE J Biomed Health Inform. 2019;23(4):1385–91.
21. Moura N, Veras R, Aires K. ABCD rule and pre-trained CNNs for melanoma diagnosis. Multimed Tools Appl. 2019;78(6):6869–88.
22. Hirano G, Nemoto M, Kimura Y, Kiyohara Y, Koga H, Yamazaki N, et al. Automatic diagnosis of melanoma using hyperspectral data and GoogLeNet. Skin Res Technol. 2020;26(6):891–7.
23. Acosta MFJ, Tovar LYC, Garcia-Zapirain MB, Percybrooks WS. Melanoma diagnosis using deep learning techniques on dermatoscopic images. BMC Med Imaging. 2021;21(1):1–11.
24. MacQueen J. Some methods for classification and analysis of multivariate observations. Paper presented at: Proceedings of the fifth Berkeley symposium on mathematical statistics and probability; 1967; University of California, Los Angeles.
25. Lloyd S. Least squares quantization in PCM. IEEE Trans Inf Theory. 1982;28(2):129–37.
26. Smith AR. Color gamut transform pairs. ACM Siggraph Comput Graphics. 1978;12(3):12–9.
27. Caselles V, Kimmel R, Sapiro G. Geodesic active contours. Int J Comput Vision. 1997;22(1):61–79.
28. Kasmi R, Mokrani K, Rader R, Cole J, Stoecker W. Biologically inspired skin lesion segmentation using a geodesic active contour technique. Skin Res Technol. 2016;22(2):208–22.
29. Jaisakthi SM, Mirunalini P, Aravindan C. Automated skin lesion segmentation of dermoscopic images using GrabCut and k-means algorithms. IET Comput Vision. 2018;12(8):1088–95.
30. Sreelatha T, Subramanyam M, Prasad MG. Shape and color feature based melanoma diagnosis using dermoscopic images. J Ambient Intell Humaniz Comput. 2020;12:5371–80.
31. Maiti A, Shekhargiri H, Chatterjee B, Rajinikanth V, Shi F, Dey N. Classification of melanoma through fused color features and deep neural networks. Inf Technol Intell Transp Syst. 2020;323:86.
32. Achanta R, Shaji A, Smith K, Lucchi A, Fua P, Süsstrunk S. SLIC superpixels compared to state-of-the-art superpixel methods. IEEE Trans Pattern Anal Mach Intell. 2012;34(11):2274–82.
33. Celebi ME, Kingravi HA, Aslandogan YA, Stoecker WV. Detection of blue-white veil areas in dermoscopy images using machine learning techniques. Paper presented at: Medical Imaging 2006: Image Processing; 2006; San Diego, CA.
34. Kira K, Rendell LA. A practical approach to feature selection. In: Machine learning proceedings 1992. Berlin, Germany: Elsevier; 1992. p. 249–56.
35. Stanley RJ, Stoecker WV, Moss RH. A relative color approach to color discrimination for malignant melanoma detection in dermoscopy images. Skin Res Technol. 2007;13(1):62–72.
36. Lingala M, Stanley RJ, Rader RK, et al. Fuzzy logic color detection: blue areas in melanoma dermoscopy images. Comput Med Imaging Graph. 2014;38(5):403–10.

37. Pathan S, Aggarwal V, Prabhu KG, Siddalingaswamy P. Melanoma detection in dermoscopic images using color features. Biomed Pharm J. 2019;12(1):107–15.
38. Celebi ME, Zornberg A. Automated quantification of clinically significant colors in dermoscopy images and its application to skin lesion classification. IEEE Syst J. 2014;8(3):980–4.
39. Barata C, Celebi ME, Marques JS. Development of a clinically oriented system for melanoma diagnosis. Pattern Recognit. 2017;69:270–85.

How to cite this article: Oukil S, Kasmi R, Mokrani K, García-Zapirain B. Automatic segmentation and melanoma detection based on color and texture features in dermoscopic images. Skin Res Technol. 2022;28:203–211. https://doi.org/10.1111/srt.13111